Available at www.sciencedirect.com

ScienceDirect

journal homepage: www.elsevier.com/locate/he

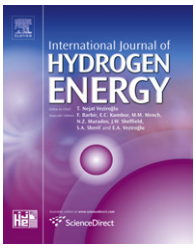

Nitrogen-doped carbon nanotubes with high activity for oxygen reduction in alkaline media

Hui Li [a], *Hao Liu* [b], *Zöe Jong* [a], *Wei Qu* [a], *Dongsheng Geng* [b], *Xueliang Sun* [b,*], *Haijiang Wang* [a,**]

[a] *Institute for Fuel Cell Innovation, National Research Council Canada, Vancouver, B.C., Canada V6T 1W5*
[b] *Department of Mechanical and Material Engineering, University of Western Ontario, London, ON, Canada N6A 5B9*

ARTICLE INFO

Article history:
Received 18 August 2010
Received in revised form
1 November 2010
Accepted 9 November 2010
Available online 9 December 2010

Keywords:
Alkaline electrolyte
Alkaline hydrogen fuel cells
Catalyst
Metal-air battery
Nitrogen-doped carbon nanotube (NCNT)
Oxygen reduction reaction (ORR)

ABSTRACT

Nitrogen-doped carbon nanotubes (NCNTs) were prepared using a floating catalyst chemical vapour deposition method. The multiwalled NCNT contains 8.4 at% nitrogen and has a dimension of 100 nm in the diameter and 10–20 nm in the wall thickness. The catalytic activity and durability of the NCNTs towards oxygen reduction reaction (ORR) were evaluated by cyclic voltammetry (CV) and rotating ring-disk electrode (RRDE) techniques in KOH solution. In addition, the effects of KOH concentration on several ORR performance indicators of the NCNT catalyst, such as the number of electrons transferred, the diffusion-limiting current density, the onset and half-wave potentials, were also examined in electrolytes of various KOH concentrations, ranging from 0.1 to 12 M. Experimental results show that NCNTs exhibited comparable activity for ORR in alkaline electrolyte as compared with commercially available Pt/C catalyst, and much higher activity than commercial Ag/C catalysts. In addition, the NCNTs showed good stability from the potential cycling test, and the concentration of KOH had significant impact on the ORR performance indicators of the NCNT catalysts.

1. Introduction

The catalytic ORR has attracted increasing attention due to its technological importance in alkaline hydrogen fuel cells, where the ORR is much faster than in the acidic media of PEM fuel cells. However, the commercialization of alkaline fuel cells is still hindered by several factors, including the insufficient kinetics of for ORR, high cost of noble metal catalysts, and the poor stability of the catalyst in alkaline media. Thus, it is of great importance to develop a low-cost, stable and more active electrocatalysts for the ORR in alkaline hydrogen fuel cells.

There have also been resurging interests in metal-air batteries, particularly lithium-air and zinc-air batteries due to the growing interests in clean energy technologies. Metal-air batteries have various important advantages, including high theoretical voltage, high theoretical energy and power densities [1–4], low operating temperature, low cost, and material recyclability. More importantly, metal-air batteries are unique compared with other batteries in that the cathode electroactive material (oxygen) is not stored in the battery system, but is supplied from the surrounding environment during the discharge process [5,6]. This unique feature simplifies the metal-air battery design, which leads to a lighter and more compact battery thus increasing the specific energy. As

* *Corresponding author*. Tel.: +1 519 661 3020.
** *Corresponding author*. Tel.: +1 604 221 3038.
E-mail addresses: xsun@eng.uwo.ca (X. Sun), haijiang.wang@nrc.gc.ca (H. Wang).
0360-3199/$ – see front matter
doi:10.1016/j.ijhydene.2010.11.025

a result, metal-air batteries are regarded as promising means of storing energy in applications where specific energy and cost are key parameters [7].

Despite the advantages, metal-air batteries have a major disadvantage of limited power output, due to the inadequate performance of air electrodes [8]. The function of air electrodes in metal-air batteries is to permit atmospheric oxygen to react electrochemically at electrocatalytic sites. The air electrode is designed to contain hydrophobic channels for facilitating the diffusion of oxygen, and to provide electrocatalytic sites that are in contact with electrolyte containing dissolved oxygen. The catalyst layer must be structured to maximize the catalyst area for the oxygen reduction reaction (ORR), thus maintaining high limiting currents [5,9].

The major reason for the high polarization of air cathodes is the slow kinetics or the high activation polarization of ORR. As a result, significant efforts have been made to develop high activity and low-cost ORR catalysts. There have been three generations of ORR catalysts for metal-air batteries [10]. The first generation has been the metal oxides, among which manganese oxides have been the most widely used [11–13] and a variety of perovskite-type oxides have also been considered promising candidates [14–20]. These oxide catalysts exhibit high stability but mostly suffer from insufficient activity due to the 2-electron pathway of ORR rather than a 4-electron pathway. The second generation has been the organometallic compounds [9]. The most prominent examples of this generation include metal tetra-methoxyphenyl porphyrin (TMPP) based ORR catalysts such as CoTMPP [21–23], and FeTMPP [24,25]. These carbon-supported TMPP catalysts show good ORR activity in alkali electrolytes and are currently used in mechanically rechargeable metal-air batteries. In comparison, CoTMPP has higher electrochemical stability but promotes 2-electron ORR pathway, while FeTMPP has inferior stability but promotes direct 4-electron reduction reaction. One common approach to improve the activity and stability is to fabricate a mixture of the two to take advantages of the high stability of CoTMPP and high activity of FeTMPP [26]. In addition to the issues of insufficient activity and stability with metal-TMPP based catalysts, high cost is another prohibiting factor for their large scale applications.

The third generation, which has newly emerged thanks to the advances in novel nanoscale materials, is the nitrogen-doped carbon nanotubes (NCNT). Although carbon nanotubes (CNT) demonstrated good characteristics as catalyst supports in reducing Pt loading and improving stability of ORR catalysts for fuel cells and metal-air batteries [27–31], including their high chemical stability, good electric conductivity, enhanced mass transport capability, and high surface area [32–34], they generally exhibit poor inherent catalytic activity for ORR [35,36]. However, chemical modification of the CNT by nitrogen-doping significantly improves the ORR activity of the resulting nitrogen-doped CNTs [37–40]. Recently, using different synthesis techniques, several groups successfully synthesized NCNTs that show improved electrocatalytic activity for ORR in dilute alkaline medium (0.1–1 M KOH or NaOH) as compared with commercially available Pt/C [38,41,42].

In the previous paper of this series, we reported how to synthesize aligned NCNTs with controlled structure and morphology using a floating catalyst chemical vapour deposition method [43]. In this study, we examine the electrochemical activity and stability of these materials for ORR in alkaline media. In particular, we investigate the effect of KOH concentration on the ORR activity with KOH concentrations as high as 12 M. This is of practical importance because ORR is more favourable in alkaline electrolytes than in acidic and neutral electrolytes, and consequently, a concentrated alkaline solution, namely, 15–30 wt% KOH (3–7 M), is suitable to ensure sufficiently high ionic conductivity that is required for utilizing thick anode, especially under low-temperature operating conditions [9,44,45].

2. Experimental

2.1. Synthesis and physical characterization of the NCNTs

The synthesis of multiwalled NCNTs with a nitrogen content of 8.4 at% on carbon paper substrates was carried out by a floating catalyst chemical vapour deposition system under argon dilute gas flow with ethylene as carbon source, melamine as nitrogen source, and ferrocene as the catalyst precursor. The details regarding the synthesis were described previously [43]. Briefly, substrates were located in the centre of the reaction chamber while melamine and ferrocene were placed at the entrance of the furnace. When the chamber was heated to 950 °C the two layer mixture reached 350 °C, which is above the sublimation temperatures of ferrocene and melamine. At the same time ethylene was introduced into the system. After 15 min, the ethylene gas was turned off and the system cooled down to room temperature in the flowing Ar gas. Field-emission scanning electron microscopy (FE-SEM) and Transmission Electron microscopy (TEM) are employed to characterize these NCNTs.

2.2. Electrochemical characterizations

Electrochemical characterization was performed in a conventional three-electrode cell using the rotating ring-disk electrode (RRDE) technique. A glassy carbon (GC) disk electrode with a geometric area of 0.25 cm^2 (Pine Instruments) was used as the rotating disk electrode (RDE) on which a thin catalyst layer was coated to form a working electrode. A Pt ring separated from the GC disk by Teflon casing was used to detect the formation of H_2O_2. The counter electrode was Pt gauze, and the reference electrode was Hg/HgO. All potentials in this paper are referred to Hg/HgO electrode. First, a catalyst ink was prepared by ultrasonically dispersing 3 mg NCNT catalyst powder for 30 min in a solution consisting of 1.25 mL ethanol (Sigma–Aldrich), 20 μL DI water (18 MΩ cm, Millipore Milli-Q system) and 13.4 μL 5% Nafion® ionomer (Alfa-Aesar). The ink was then pipetted onto the glassy carbon disk surface with a catalyst loading of 100 μg cm^{-2}, forming a catalyst layer. After air-drying, this working electrode was transferred into the electrochemical cell for measurements. In addition to the NCNT, commercially available carbon-supported Pt powder (Pt/C, 46.9 wt% Pt, purchased from TKK) and carbon-supported Ag (Ag/C, 60 wt% Ag, purchased from E-TEK) were also used in

this study to make the catalyst layers for the purpose of comparison.

Second, the electrolyte KOH solution was prepared from reagent-grade KOH (Sigma–Aldrich). In this work, KOH solutions with concentrations ranging from 0.1 M to 12 M were employed to study the effect of KOH concentration on catalyst activity for ORR.

During the electrochemical measurements which were conducted at room temperature, the freshly prepared working electrode was immersed in the electrolyte, and then the electrolyte solution was deaerated by purging with nitrogen (99.999%, Praxair) for 30 min. The electrode surface was electrochemically cleaned by repeatedly cycling the potential between −0.8 and 0.5 V for more than 20 cycles at a scan rate of 100 mV s^{-1}. Surface cyclic voltammetry (CV) was then conducted with potential sweeping between −0.6 and 0.15 V at 50 mV s^{-1} in the presence of constant N_2 bubbling, and the electrode surface was determined to be clean when a reproducible voltammogram was recorded. Following the CVs in N_2, the KOH solution was saturated with oxygen (99.999%, Praxair) through constant bubbling for 30 min before a set of CVs were recorded in the presence of O_2 using the same scanning rate and same potential range as with N_2 for comparison. For ORR activity measurements, linear sweep voltammetry (LSV) was conducted between −0.6 and 0.1 V at 5 mV s^{-1} in O_2-saturated KOH solution at various rotating speeds. Simultaneously, the ring potential was held at 0.5 V, where the oxidation of H_2O_2 was under pure diffusion control, and the ring current was recorded to monitor any H_2O_2 production originating from the ORR on the disk. A higher ring current indicates a higher production yield of H_2O_2, an undesired byproduct from ORR.

3. Results and discussion on electrochemistry part

3.1. Physical characterizations

Long, dense NCNTs grown on carbon paper substrate are clearly seen from Fig. 1. The carbon paper substrate is totally covered by NCNT bundles with a length of around 100 μm. The inserted magnified SEM image shows good alignment of the

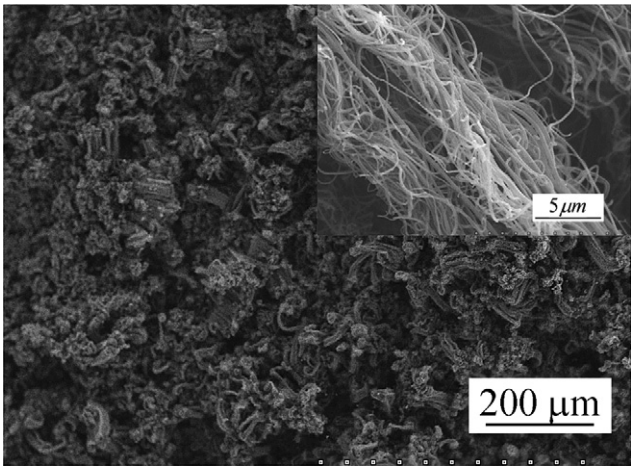

Fig. 1 – SEM images of the NCNTs.

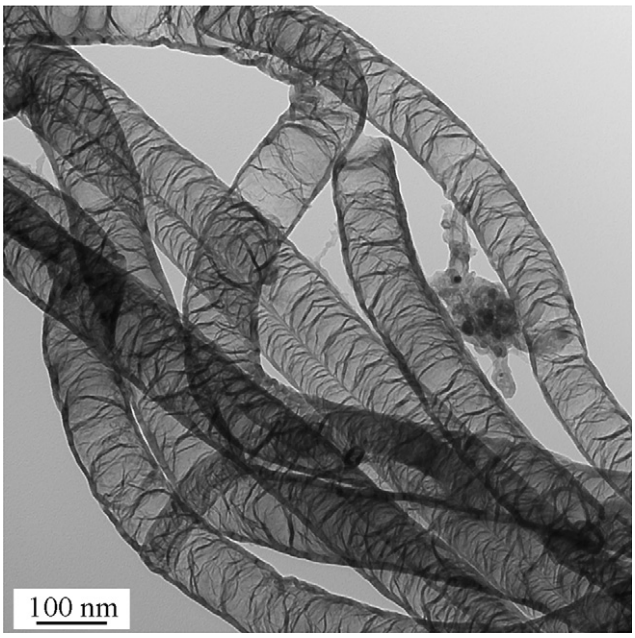

Fig. 2 – TEM image of NCNTs.

tubes within one bundle. The TEM image of these NCNTs is shown in Fig. 2(b). The NCNTs have an average diameter of 100 nm and the wall thickness is 10–20 nm. The tubes show a corrugated morphology.

3.2. Electrochemical testing

3.2.1. Cyclic voltammetry

Fig. 3 shows the CVs of the NCNT conducted in the absence (N_2 bubbling) and presence of oxygen (O_2 bubbling) at room temperature. No clear redox features can be observed in the CV with N_2, suggesting that any metal residuals that might have remained from the NCNT synthesis process were completely removed from the NCNT surface, thus not contributing to the ORR activity. The CV in O_2, on the other hand, exhibits a steep

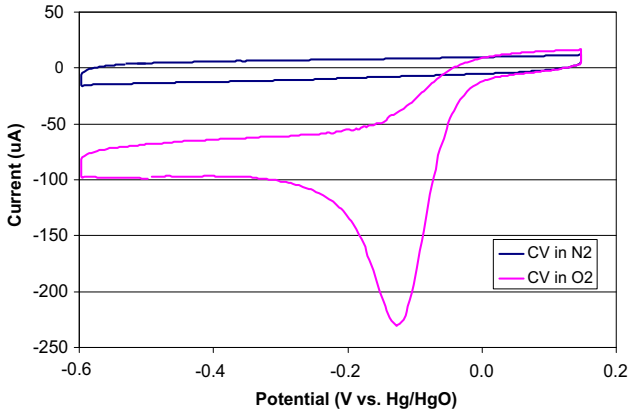

Fig. 3 – Cyclic voltammograms of the NCNT catalysts in N_2 and O_2-saturated 3 M KOH electrolyte, respectively, at room temperature. Scan rate: 50 mV s^{-1}.

increase in the oxygen reduction current, reaching a peak current at a potential of about −0.13 V vs. Hg/HgO.

3.2.2. *RRDE results (LSVs)*

To obtain further information into the kinetics of ORR, LSV technique using RRDE setup was employed to record the polarization curves that can generate significant amount of kinetic information on ORR, such as the catalyst activity measured by a current density at a given potential, selectivity of the ORR to water versus hydrogen peroxide, and the electron transfer number of ORR. In the RRDE setup, the electrolyte provides OH^- to the ORR reaction at the catalyst layer casted on the GC electrode. Oxygen within the solution diffuses to the surface of the electrode and reacts to form water preferably through a 4-electron pathway, or to produce hydrogen peroxide undesirably through a 2-electron pathway. Clearly, the diffusivity and solubility of oxygen in the KOH electrolytes can significantly contribute to the mass transfer effect of oxygen diffusion through the solution, thus affecting the current densities measured by the potentiostat at a given potential. Therefore, when evaluating the activity of the ORR catalysts, rotating the electrode at different rates is always employed to account for the mass transfer effect of oxygen diffusion so that the pure kinetic current can be calculated to provide a true measure of catalyst performance at a given potential [46].

The polarization curves of ORR with NCNT catalyst obtained at room temperature through LSV in O_2-saturated 3 M and 6 M KOH electrolytes, respectively, are presented in Fig. 4. For comparison, identical measurements were performed with commercial Pt/C (46.9 wt%) and Ag/C (60 wt%) catalysts, and the polarization curves of these two commercial catalysts are also presented in Fig. 4. Several observations can be made from Fig. 4: (1) NCNT has well-defined diffusion-limiting current plateau in both 3 M and 6 M KOH electrolytes, which means that the distribution of active sites is uniform [47,48]; (2) In 3 M KOH electrolyte, NCNT catalyst is under diffusion control at potential lower than −0.25 V, but is under mixed kinetic and diffusion control in the potential range between −0.25 and 0.0 V; in 6 M KOH electrolyte, the potential boundary between diffusion and mixed control shifts to −0.1 V; (3) NCNT exhibits a more positive onset potential than Ag/C but more negative potential than Pt/C; (4) The limiting current of NCNT is much higher than that of Ag/C but slightly lower than that of Pt/C in 3 M KOH; however, the difference of limiting currents between NCNT and Pt/C becomes insignificant in 6 M KOH, suggesting that the negative effect of higher concentration of KOH to be discussed later is much less for NCNT than for Pt/C.

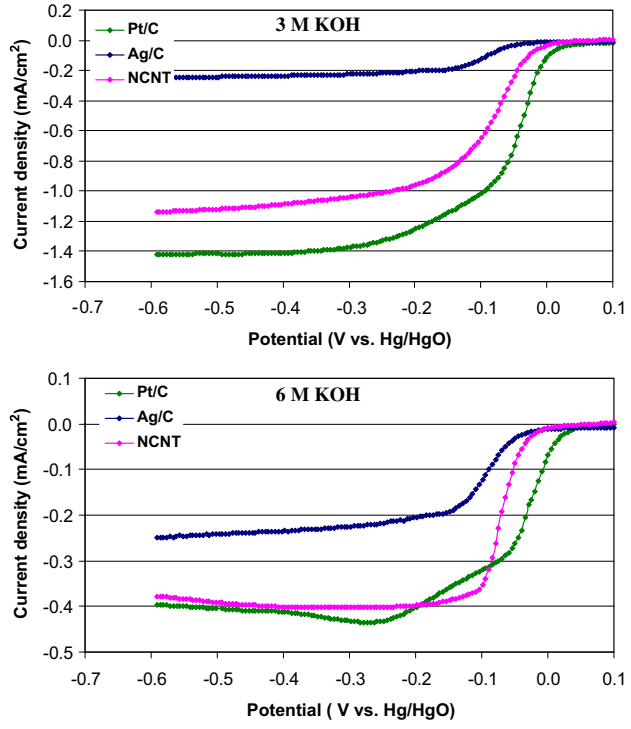

Fig. 4 – Polarization curves of NCNT in 3 M KOH (top) and 6 M KOH (bottom), respectively, at room temperature in comparison with polarization curves of Pt/C and Ag/C. Scan rate: 5 mV s^{-1}; electrode rotation rate: 1600 rpm.

The differences in activity between NCNT and commercial catalysts can also be evaluated from the Koutecky–Levich analysis. If assuming that the ORR reaction order is one for the catalysts, the Koutecky–Levich equation can be written as:

$$\frac{1}{i} = \frac{1}{i_k} + \frac{1}{i_d} \tag{1}$$

where i_k is the kinetic current density for the ORR, which is proportional to the rate of reaction and increases exponentially with overpotential [46]; i_d is the diffusion-limiting current density controlled by the mass transfer of oxygen in the solution, as expressed in Eq. (2):

$$\frac{I_d}{A} = i_d = 0.62nFC_{O_2}D_{O_2}^{2/3}\nu^{-1/6}\omega^{1/2} \tag{2}$$

where I_d is the disk plateau current (diffusion-limiting current), A is the electrode diffusion area, n is the overall number of transferred electrons in the ORR process, F is the Faradaic constant, C_{O_2} is the oxygen concentration (solubility) in the electrolyte, D_{O_2} is the oxygen diffusion coefficient, υ is the kinematic viscosity of the electrolyte, and ω is the electrode rotation rate.

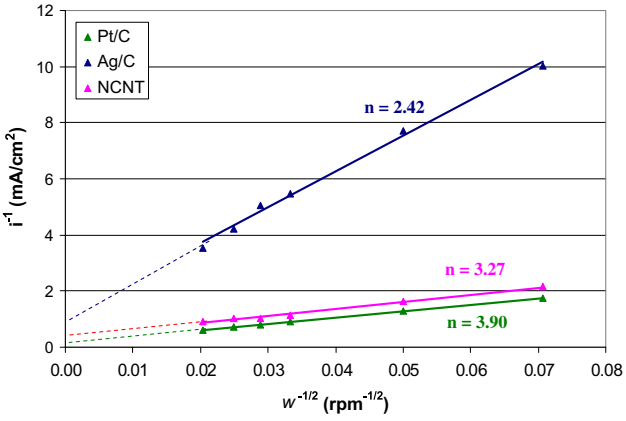

Fig. 5 – Koutecky–Levich plots for NCNT, commercial Pt/C (46.9 wt%) and Ag/C (60 wt%) catalysts in 3 M KOH at a potential of −0.4 V vs. Hg/HgO.

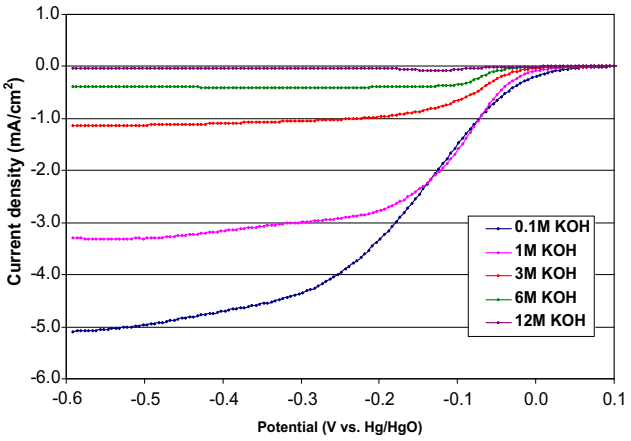

Fig. 6 – Polarization curves for the ORR on the NCNT catalyst in oxygen-saturated electrolyte solutions containing 0.1, 1.0, 3.0, 6.0, and 12 M KOH. Scan rate: 5 mV s^{-1}; electrode rotation rate: 1600 rpm.

Substituting Eq. (2) into Eq. (1), Koutecky–Levich equation can be rewritten as:

$$\frac{1}{i} = \frac{1}{i_k} + \frac{1}{B\omega^{\frac{1}{2}}} \tag{3}$$

$$B = 0.62nFC_{O_2}D_{O_2}^{2/3}\nu^{-1/6} \tag{4}$$

where B is the Levich slope. Koutecky–Levich plots at −0.4 V in 3 M KOH electrolyte for NCNT and the two commercial catalysts are illustrated in Fig. 5, which also includes the electron transfer number calculated for each catalyst. It is seen that ORR on NCNT is mainly a 4-electron reduction process, similarly with that on Pt/C, but the ORR on Ag/C is clearly a 2-electron process. In addition, the Koutecky–Levich plots for NCNT and Pt/C have similar intercepts that are slighter higher than 0, but the intercept for Ag/C is much higher than 0. Since the non-zero intercept of Koutecky–Levich plot demonstrates the presence of kinetic limitations [46,49], it can be concluded that NCNT is kinetically comparable to Pt/C catalyst but much faster than Ag/C catalyst for ORR. The comparable catalytic activity of NCNT with commercial Pt/C has significantly important practical implications if we compare the material costs of the two catalysts for large-scale commercialization.

3.2.3. *Effect of KOH concentrations*

For practical application purposes, we studied the activity of NCNT for ORR in electrolytes containing various concentrations of KOH with an aim to see how the catalyst activity changes with increasing KOH concentration. Fig. 6 shows the polarization curves at 1600 rpm as a function of KOH concentration obtained by RRDE tests at room temperature. As seen from Fig. 6, the increased KOH concentration resulted in not only the shifting of the onset potential to more negative

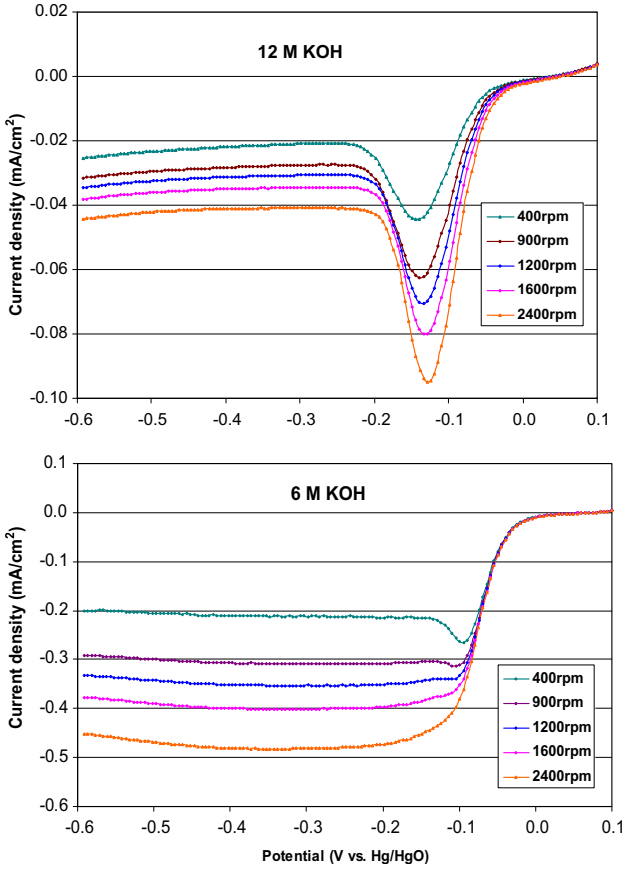

Fig. 7 – Polarization curves for the ORR on the NCNT catalyst in oxygen-saturated 6 M and 12 M KOH electrolytes at various rotation rates. Scan rate: 5 mV s^{-1}.

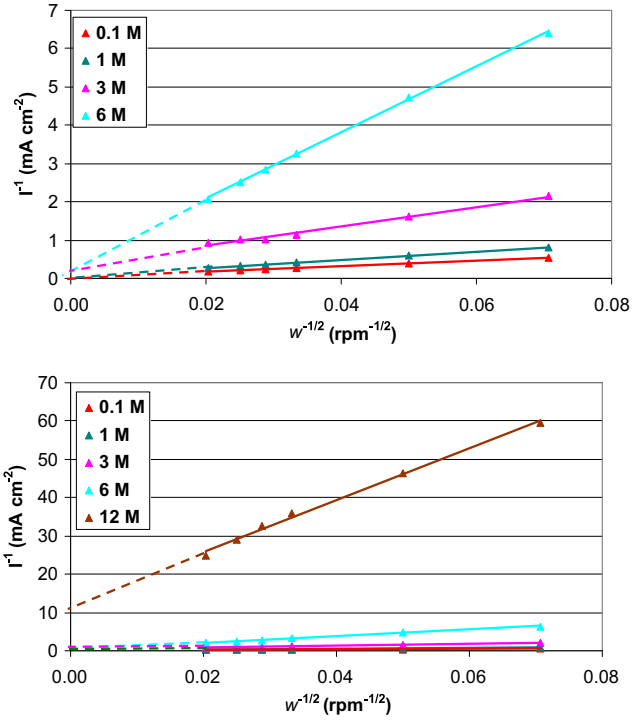

Fig. 8 – Koutecky–Levich plots for NCNT catalysts in various concentrations of KOH at a potential of −0.4 V vs. Hg/HgO.

Table 1 – Summary of the performance indicators of NCNT catalyst for ORR.

[KOH] (M)	Electron transfer number at 1600 rpm	Limiting current density (mA/cm^2)[a]	Half-wave potential (V)[b]	Onset potential (V)
0.1	3.70	−4.71	−0.144	0.040
1	3.44	−3.16	−0.099	0.025
3	3.27	−1.09	−0.084	0.015
6	3.42	−0.40	−0.070	0.010
12	2.99	−0.04	−0.061	−0.022

a Limiting current measured at −0.4 V vs. Hg/HgO and 1600 rpm.
b Half-wave potential measured at 1600 rpm.

values but also the decrease of current densities at all regions - kinetic region, mixed region and diffusion-limiting region. In particular, when the KOH concentration increased from 0.1 M to 12 M, the diffusion-limiting current density at −0.4 V was reduced from 4.71 to 0.04 mA cm^{-2}, showing more than 100 times reduction. The magnitude of reduction in limiting current density is slightly smaller than that of the reduction of oxygen solubility from 1.21×10^{-6} mol cm^{-3} in 0.1 M KOH to 1.01×10^{-6} mol cm^{-3} in 12 M KOH [50,51].

Also shown in Fig. 6, as KOH concentration increased to 12 M, the polarization curve exhibited peak current density before it plateaued at the diffusion-limiting current density. The presence of peak current densities in LSV graphs was associated with the low solubility of oxygen in highly concentrated KOH solution and has never been reported in the literature since the most commonly used alkaline media has been 0.1 M KOH [38,39,41,42]. The presence of peak current densities in polarization curves (LSV graphs) is better demonstrated in Fig. 7 which illustrates the polarization curves in highly concentrated KOH electrolytes (6 and 12 M KOH) as a function of rotating rate, both obtained by RRDE tests at room temperature. In 6 M KOH electrolyte, the polarization curves started to have peak current densities after the rotating rate was lower than 1200 rpm, but in 12 M KOH electrolyte, regardless of the rotation speed, all of the polarization curves showed peak current densities.

Fig. 8 presents the Koutecky–Levich plots obtained at −0.4 V for different concentrations of KOH. It shows that, as the KOH concentration increased, not only the K–L slopes increased significantly, which indicated the decrease in the number of electrons transferred in ORR and thus the reduction in H_2O selectivity, but also the Y-intercepts of the K–L plots became much greater than 0, suggesting a decreasing kinetics of the-catalyst for ORR. Table 1 summarizes the performance indicators of NCNT catalysts in electrolytes of various KOH concentrations, including the number of electrons transferred in ORR, the diffusion-limiting current density, the half-wave potential (HWP), and the onset potential obtained at −0.4 V vs. Hg/HgO with a rotating rate of 1600 rpm. It is clear that the catalyst activity was significantly compromised by the low concentration of oxygen in highly concentrated KOH solutions, despite the benefit of increased conductivity. This has important implications for the design of the air cathodes in metal-air batteries in that the air cathodes have to be designed to facilitate the easy access for air diffusion to the catalyst active sites, and optimizations need to be conducted in the use of highly concentrated KOH considering both the benefits of elevated conductivity and the disadvantages of lowered solubility of oxygen in the electrolyte.

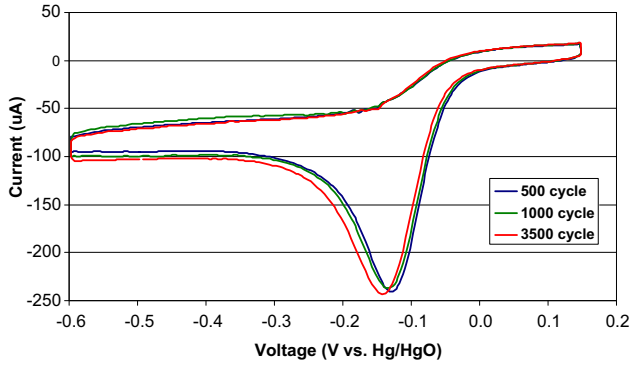

Fig. 9 – Stability test. CVs for the ORR with NCNT catalyst in oxygen-saturated 3 M KOH solution at room temperature. Scan rate: 50 mV s^{-1}.

It should be pointed out that, although both Gong et al. [41] and Nagaiah et al. [42] reported much better performance of their NCNT catalysts over commercial Pt/C catalysts in their respective studies, the diffusion-limiting currents in their work were obtained in dilute alkaline media (0.1 M KOH and 1 M NaOH, respectively) and reported to be around 0.80 mA and 0.15 mA, in comparison to 1.18 mA and 0.79 mA achieved in our work in 0.1 M and 1 M KOH, respectively.

3.2.4. *Stability*

Stability test for the NCNT catalyst was conducted by running continuous potential cycling between −0.6 and +0.15 V in oxygen-saturated 3 M KOH solution for 3500 cycles. As can be seen from Fig. 9, the NCNT catalyst shows almost identical voltammetric graphs before and after the continuous potential cycling.

Thus, it can be seen that NCNT exhibited good ORR activity and stability in alkaline solution. Although currently the active site of NCNT cannot be identified clearly, many researchers have considered that graphene-coordinated FeN_4 or FeN_2 moieties are the active sites [52–54]. However, some researchers do not agree with the view; Ozkan et al. think that the higher activity of N-doped carbon fibers should be related to edge plane exposure, and not necessarily to the presence of metal residues [40]. And Dai et al. [41] suggested that the strong electronic affinity of the nitrogen atoms and the substantially high positive charge density on the adjacent carbon atoms should also contribute to the catalytic activity. Although no residual Fe was detected from the CV graphs

shown in Fig. 3, more study is recommended to clearly identify the active site of NCNT [43].

4. Conclusions

Multiwalled NCNTs with a nitrogen content of 8.4 at%, and a dimension of 100 nm in the diameter and 10–20 nm in the wall thickness were synthesized using a floating chemical vapour deposition technique. The electrochemical activities of these NCNTs towards ORR, characterized by CV and RRDE techniques in alkaline solutions containing various concentrations of KOH (0.1–12 M), showed comparable values as compared with commercial Pt/C catalyst, and much higher values than commercial Ag/C catalysts. In addition, the NCNT catalysts were also evaluated for their stability by potential cycling in the presence of oxygen, and the NCNT catalyst did not experience noticeable changes after 3500 cycles. In light of the strong need to develop alternative catalysts to replace Pt based catalysts, and in consideration of the additional benefits of the superior mechanical and thermal properties of carbon nanotube materials, NCNTs definitely hold the promises of being the inexpensive, highly active, and durable ORR electrocatalysts for large-scale commercialization of metal-air batteries.

Acknowledgements

This work is financially supported by National Research Council of Canada, Institute of Fuel Cell Innovation and University of Western Ontario.

REFERENCES

[1] Neng L, Xiaioming Y, Wanjing Z, Bingxiong L. Electrocatalytic activity of spinel-type oxides $LiMn_{2-x}Co_xO_4$ with large specific surface areas for metal–air battery. J Power Sources 1998;74:255–8.
[2] Zidong W, Wenzhang H, Shengtal Z, Jun T. Carbon-based air electrodes carrying MnO_2 in zinc–air batteries. J Power Sources 2000;91:83–5.
[3] Wi-kang H, Zhou Y, Dag N. Influence of MH electrode thickness and packing density on the electrochemical performance of air–MH batteries. J Power Sources 2001;102:35–40.
[4] Maya M, Orecchia C, Strano M, Tosco P, Vanni M. Effect of structure on the electrical performance of gas diffusion electrodes for metal air batteries. Electrochim Acta 2000;46:423–32.
[5] Blurton KF, Sammells AF. Metal/air batteries: their status and potential – a review. J Power Sources 1979;4:263–79.
[6] Williford RE, Ji-Guang Z. Air electrode design for sustained high power operation of Li–air batteries. J Power Sources 2009;194:1164–70.
[7] Smedley S, Zhang XG. Zinc–air: hydraulic recharge. In: Garche J, editor. Incyclopaedia of electrochemical power sources. Oxford UK: Elsevier; 2010. p. 393–403.
[8] Arai H, Hayashi M. Zinc-air. In: Garche J, editor. Incyclopaedia of electrochemical power sources. Oxford UK: Elsevier; 2010. p. 55–61.
[9] Arai H, Hayashi M. Secondary batteries: metal-air systems. In: Garche J, editor. Incyclopaedia of electrochemical power sources. Oxford UK: Elsevier; 2010. p. 347–55.
[10] Vladimir N, Haijiang W, Jonathan JM, Wei Q. A review on air cathodes for zinc–air fuel cells. J Power Sources 2010;195:1271–91.
[11] Kanungo SB, Parida KM, Sant BR. Studies on MnO_2-III. The kinetics and the mechanisms for the catalytic decomposition of H_2O_2 over different crystalline modifications of MnO_2. Electrochim Acta 1986;26:1157–67.
[12] Liompart L, Yu LT, Mas JC, Mendiboure A, Vignaud R. Oxygen-regeneration of discharged manganese dioxide electrode. J Electrochem Soc 1990;137:371–7.
[13] Brenet JP. Electrochemical behaviour of metallic oxides. J Power Sources 1979;4:183–90.
[14] Hyodo T, Hayashi M, Miura N, Yamazoe N. Catalytic activities of rare-earth manganites for cathodic reduction of oxygen in alkaline solution. J Electrochem Soc 1996;143:L266–7.
[15] Hyodo T, Hayashi M, Mitsutake S, Miura N, Yamazoe N. Praseodymium–calcium manganites (Pr1-xCaxMnO3) as electrode catalyst for oxygen reduction in alkaline solution. J Appl Electrochem 1997;27:745–9.
[16] King WJ, Tseung AC. The reduction of oxygen on nickel-cobalt oxides-I: the influence of composition and preparation method on the activity of nickel-cobalt oxides. Electrochim Acta 1974;19:485–91.
[17] Xiaoxia L, Aaron LZ, Wei Q, Haijiang W, Rob H, Lei Z, et al. Magneli phase Ti_4O_7 electrode for oxygen reduction reaction and its implication for zinc-air rechargeable batteries. Electrochim Acta 2010;55:5891–8.
[18] Yang CC. Preparation and characterization of electrochemical properties of air cathode. Int J Hydrogen Energ 2004;29:135–43.
[19] Yang CC, Hsu ST, Chien WC, Shih MC, Chiu SJ, Lee KT, et al. Electrochemical properties of air electrodes based on MnO_2 catalysts supported on binary carbons. Int J Hydrogen Energ 2006;31:2076–87.
[20] Ananth MV, Manimaran K, Raj A, Sureka N. Influence of air electrode electrocatalysts on performance of air-MH cells. Int J Hydrogen Energ 2007;32:4267–71.
[21] Ovshinsky SR, Fierro C, Reichman B, Mays W, Strebe J, Fetcenko MA, et al. US Patent 7,097,933; 2003.
[22] Gojkovic SL, Gupta S, Savinell RF. Heat-treated iron (III) tetramethoxyphenyl porphyrin supported on high-area carbon as an electrocatalyst for oxygen reduction. J Electrochem Soc 1998;145:3493–9.
[23] Aaron LZ, Haijiang W, Wei Q, Xiaoxia L, Zoe J, Hui L. Low temperature pyrolyzed cobalt tetramethoxy phenylporphyrin catalyst and its applications as an improved catalyst for metal air batteries. J Power Sources 2010;195:5587–95.
[24] Deryn C, Rongzhong J. Novel electrocatalysts for direct methanol fuel cells. SolidState Ionics 2002;148:591–9.
[25] Lefèvre M, Dodlet JP, Bertrand P. O_2 reduction in PEM fuel cells: activity and active site structural information obtained by the pyrolysis at high temperature of Fe precursors. J Phys Chem B 2000;104:11238–47.
[26] Shaojun D, Baifeng L, Junli L, Nagao K. Cobalt octa-ethyl-tetrapyrazino-porphyrazine: spectroscopy, and electrocatalytic and kinetic study of oxygen reduction at a glassy carbon electrode. J Porphyrins Phtralocyannies 1997;1:33–4.
[27] Francisco RR. The role of carbon materials in heterogeneous catalysis. Carbon 1998;36:159–75.
[28] Shao-Wei B, Zhuo M, Wei-Guo S. Preparation and characterization of carbon nitride nanotubes and their applications as catalyst supporter. J Phys Chem C 2009;113:8668–72.
[29] Cheng W, Mahesh W, Xin W, Jason MT, Robert CH, Yushan Y. Proton exchange membrane fuel cells with carbon nanotube based electrodes. Nano Lett 2004;4:345–8.

[30] Yuyan S, Jun L, Yong W, Yuehe L. Novel catalyst support materials for PEM fuel cells: current status and future prospects. J Mater Chem 2009;19:46–59.
[31] Yuyan S, Jiehe S, Geping Y, Yunzhi G. Nitrogen-doped carbon nanostructures and their composites as catalytic materials for proton exchange membrane fuel cell. Appl Catal B 2008; 79:89–99.
[32] Sumio L. Helical microtubules of graphitic carbon. Nature 1991;354:56–8.
[33] Wenzhen L, Changhai L, Lieshan Q, Wijian Z, Hongmei H, Zhaobin W, et al. Carbon nanotubes as support for cathode catalyst of a direct methanol fuel cell. Carbon 2002;40: 791–4.
[34] Pichumani JB, Kalathur SVS, Angel R, Julio AA, Pulickel MA. Improved charge transfer at carbon nanotube electrodes. Adv Mater 1999;11:154–7.
[35] Yeager E. Dioxygen electrocatalysis: mechanisms in relation to catalyst structure. J Mol Catal 1986;38:5–25.
[36] Chen CY, Yang P. Performance of an air-breathing direct methanol fuel cell. J Power Sources 2003;123:37–42.
[37] Maldonado S, Stevenson KJ. Influence of nitrogen doping on oxygen reduction electrocatalysis at carbon nanofiber electgrodes. J Phys Chem B 2005;109:4707–16.
[38] Zhu C, Drew H, Haisheng T, Ryan SH, Zhongwei C. Highly active nitrogen-doped carbon nanotubes for oxygen reduction reaction in fuel cell applications. J Phys Chem C 2009;113:21008–13.
[39] Zhu C, Drew H, Zhongwei C. Nitrogen doped carbon nanotubes and their impact on the oxygen reduction reaction in fuel cells. Carbon 2010;48:3057–65.
[40] Matter PH, Wang E, Arias M, Biddinger EJ, Ozkan US. Oxygen reduction reaction activity and surface properties of nanostructured nitrogen-containing carbon. J Mol Catal A Chem 2007;264:73–81.
[41] Kuanping G, Feng D, Zhenhai X, Michael D, Liming D. Nitrogen-doped carbon nanotube arrays with high electrocatalytic activity for oxygen reduction. Science 2009; 323:760–4.
[42] Tharamani CN, Shankhanmala K, Michael B, Martin M, Wolfgang S. Nitrogen-doped carbon nanotubes as a cathode catalyst for the oxygen reduction reaction in alkaline medium. Electrochem Commun 2010;12:338–41.
[43] Hao L, Yong Z, Ruying L, Xueliang S, Sylvian D, Hakima AR, et al. Structural and morphological control of aligned nitrogen-doped carbon nanotubes. Carbon 2010;48:1498–507.
[44] Haas O, Wesemael JV. Zinc-air: electrical recharge. In: Garche J, editor. Incyclopaedia of electrochemical power sources. Oxford UK: Elsevier; 2010. p. 384–92.
[45] Kinoshita K. Electrochemical oxygen technology. New York: John Wiley & Sons Inc; 1992.
[46] Matter PH, Ling Z, Umit SO. The role of nanostructure in nitrogen-containing carbon catalysts for the oxygen reduction reaction. J Catal 2006;239:83–96.
[47] Sepa DB, Vojnovic MV, Damjanovic A. Reaction intermediates as a controlling factor in the kinetics and mechanism of oxygen reduction at platinum electrodes. Electrochim Acta 1981;26:781–93.
[48] Gojkovic SL, Gupta S, Savinell RF. Heat-treated iron (III) tetramethoxyphenyl porphyrin chloride supported on high-area carbon as an electrocatalyst for oxygen reduction: part II. Kinetics of oxygen reduction. J Electroanal Chem 1999;462: 63–72.
[49] Hui-Juan Z, Qi-Zhong J, Lianliang S, Xianxia Y, Zi-Feng M. Influence of heat treatment on the activity and structure of CoTETA/C catalysts for oxygen reduction reaction. Electrochim Acta 2010;55:1107–12.
[50] Gubbins KE, Walker RD. The solubility and diffusivity of oxygen in electrolytic solutions. J Electrochem Soc 1965;112:469–71.
[51] Davis RE, Horvath GL, Tobias CW. The solubility and diffusion coefficient of oxygen in potassium hydroxide solutions. Electrochim Acta 1967;12:287–97.
[52] Bouwkamp-Wijnoltz AL, Visscher W, Van Veen JAR, Boellaard E, Van der Kraan AM, Tang SC. On active-site heterogeneity in pyrolyzed carbon-supported iron porphyrin catalysts for the electrochemical reduction of oxygen: an in situ Mossbauer study. J Phys Chem B 2002; 106:12993–3001.
[53] Lefèvre M, Proietti E, Jaouen F, Dodelet JP. Iron-based catalysts with improved oxygen reduction activity in polymer electrolyte fuel cells. Science 2009;324:71–4.
[54] Ulrike IK, Irmgard AW, Sebastian F, Peter B. Nature of the catalytic centers of porphyrin-based electrocatalysts for the ORR: a correlation of kinetic current density with the site density of Fe–N_4 centers. J Phys Chem C 2008;112:15356–66.